Measured dynamics of a thin cylindrical shell subject to axial excitation

James A. Forrest

Maritime Platforms Division, Defence Science & Technology Organisation, PO Box 4331, Melbourne VIC 3001, Australia.
Email: james.forrest@dsto.defence.gov.au

ABSTRACT

One source of structural vibration in a submarine is the fluctuating axial thrust force applied to the thrust block by the propeller shaft. This paper describes the initial stages of experimental work being undertaken to validate an existing mathematical model for the sound radiation from a submarine excited by this mechanism. A thin cylindrical shell 1500mm long and 400mm in diameter made of 2mm thick steel with its ends capped by 20mm thick steel discs is examined. The shell was suspended from eyelets welded at either end and was excited axially by a modal shaker mounted inside the cylinder on one of the end caps. The first few modes with significant axial content were extracted from frequency-response functions measured at a number of points on the surface of the cylinder and the end caps and are described. This work will lead into the development of a sound radiation model suitable for use in the active vibration control of the cylinder.

INTRODUCTION

The prediction and control of sound radiated from submarines is a subject of perennial interest to navies around the world. Minimisation of radiated sound is essential to reduce the detectability of a submarine and thereby maximise its effectiveness. A common approach is to base investigations on relatively simple cylindrical shell structures. Much early work on shells and cylindrical shells in particular is summarised by Leissa (1993). Hodges et al. (1985a) present a detailed model for vibration transmission in a ribbed cylinder that also models the internal degrees of freedom and resonances of the ribs; they compare this model to a range of measurements on a ribbed cylinder (Hodges et al. 1985b). The wave propagation in periodically stiffened shells, with its pass and stop bands, is modelled using a finite-element approach by Solaroli et al. (2003) and by an analytical technique by Lee and Kim (2002). It is an interesting fact that there is no single agreed upon theory for the vibration of thin shells. Ruotolo (2002) investigates the effect of using the slightly differing theories of Love, Donnell, Flügge and Sanders to calculate the interior noise level of ring-stiffened cylinders representing aircraft fuselages.

Heavy fluid loading, such as that presented by water surrounding a submerged vessel, markedly alters the response of a structure. Rumerman (2002) investigates the effect of fluid loading on the radiation efficiency of flat panels. Sandman (1976) determines the fluid-loading influence coefficients for a finite submerged plain cylindrical shell to account for this effect. Scott (1988) presents a comprehensive analysis of the free modes of propagation for an infinitely long thin cylindrical shell with fluid loading, developing individual expressions for the higher order terms in the shell equations to better suit the analysis approach. Another analytical study that looks into the acoustic radiation from the shell as well is given by Harari and Sandman (1990). Choi et al. (1995) use a modal-based method to model the vibration and acoustic radiation of submerged cylindrical shells that include internal substructures.

Finite-element (FE) approaches can model more general structures than can be treated by analytical means. Marcus and Houston (2002) use an FE model to show that the addition of point masses to the internal frames of a submerged cylindrical shell increase its acoustic radiation by coupling high and low order circumferential resonances. Homm et al. (2003a) use both FE analysis alone and FE combined with the boundary-element (BE) method to model the structural and acoustic response of a complicated structure consisting of two hemispherically capped cylinders with different radii joined together and containing some internal structure. Comparison to underwater measurements of the structure (Homm et al. 2003b) shows that the combined FE-BE approach is superior. At higher frequencies, FE methods become impracticable, and methods such as statistical energy analysis (SEA) can be used. Blakemore et al. (1999) model a fluid-loaded ribbed cylindrical shell with an extended form of SEA that can deal with the periodicity of the structure.

Various techniques for the active control of vibration, including active structural acoustic control (ASAC), are given in Fuller et al. (1996). Ideally, active control seeks to minimise a measured error signal. However, in the case of a submarine, the quantity to be minimised is the far-field radiated sound, while the quantity that can be measured is the hull vibration. Thus a cost function is required, that relates the hull vibration to the radiated sound, and it is this function that must be minimised by the control system. Such a cost function must be computationally efficient to be implemented in a real-time control system. This rules out directly using numerically intensive radiation models such as those based on FE methods. A simplified analytical radiation model is described in Pan et al. (2005), based on a formulation given by Junger and Feit (1972) for a thin cylindrical shell. It considers low-frequency axial excitation, as might be induced by the propeller shaft on the thrust block of a submarine, such that the hull stiffeners can be taken to be a smeared effect of increasing the stiffness and mass of a uniform shell. Only axisymmetric motion is considered (i.e. $n = 0$, see the next section). This paper presents the first stages of an experimental investigation that seeks to test the validity of this model. It is expected that the cylindrical shell investigated will eventually act as the test bed for various active vibration control techniques, including the use of piezo stacks to provide a controlling moment to a rib stiffener as

described in the theoretical study of Pan et al. (2005), and the use of inertial actuators to provide controlling forces.

THEORETICAL BACKGROUND

Figure 1 shows a uniform thin cylindrical shell of radius *a*, thickness *h* and length *L*. Also shown is the coordinate system *x* (longitudinal), *y* (tangential) and *z* (radial) centred on an element of the shell surface which is at angular position θ.

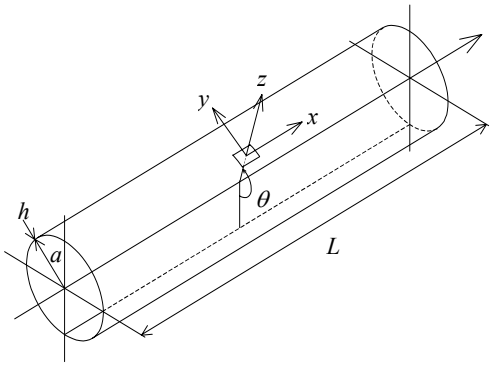

Figure 1. A thin cylindrical shell of radius *a* and thickness *h* showing the local coordinate system *x*, *y* and *z* used for (1).

The equations of motion for the free vibration of the thin cylindrical shell of Figure 1, according to the Donnell-Mushtari theory, are (Leissa, 1993)

$$\begin{aligned} &a^2u_{xx} + (1-\nu)u_{\theta\theta}/2 - \rho(1-\nu^2)a^2\ddot{u}/E + (1+\nu)av_{x\theta}/2 + \nu a w_x = 0 \\ &(1+\nu)a\,u_{x\theta}/2 + (1-\nu)a^2v_{xx}/2 + v_{\theta\theta} - \rho a^2(1-\nu^2)\ddot{v}/E + w_\theta = 0 \\ &\nu a u_x + v_\theta + w + h^2\nabla^4 w/12a^2 + \rho a^2(1-\nu^2)\ddot{w}/E = 0 \end{aligned} \qquad (1)$$

where *u*, *v* and *w* are the displacements in the *x*, *y* and *z* directions respectively; ρ is the density, *E* the Young's modulus and ν the Poisson's ratio of the shell material; and subscripts *x* and θ denote differentiation with respect to those variables, while dot denotes differentiation with respect to time. While other thin-shell theories such as those of Flügge and Sanders include more terms than in equations (1) to better model the bending effects in shells with higher thickness-to-radius ratios, even these simplest equations illustrate the high degree of coupling between the three displacements *u*, *v* and *w*. Thus radial displacement, which is the main source of sound radiated from the shell, can be excited even when the only excitation is axial.

For a finite shell with shear diaphragm end conditions, which equate to "simple support", the longitudinal variation of the radial displacement would be assumed to be described by $\sin(m\pi x/L)$ terms, where the positive integer *m* is the number of half waves that fit along the length *L*. Although the cylinder to be considered has shell end conditions that fall somewhere between shear diaphragm and fully clamped so that this simple term is no longer strictly valid, the number of half waves is still a useful way to think of the mode shapes. Likewise, the circumferential variation of the three displacement components can be described by $\sin n\theta$ and $\cos n\theta$ terms, where *n* is the number of full waves developed around the circumference. Therefore, the modes of the cylinder can be described in terms of *m* and *n* values to succinctly describe the deformed shape of the shell. The $n = 0$ case represents an expansion or "breathing" mode of the cylindrical cross-section. For a simple ring, formulas in Blevins (1995) indicate that the $n = 0$ ring mode is higher in frequency than the first few $n = 1, 2, 3\ldots$ modes. Blevins (1995) also notes that for a given *m*, the $n = 1$ cylindrical shell modes are not generally the lowest in frequency. These latter modes represent a translation of the cylinder cross-section undistorted, i.e. they are beam bending modes.

Following the results presented in Leissa (1993), the solution for the natural frequencies of a finite shell with shear-diaphragm support at each end is as follows. Assume that the displacements take the form

$$\begin{aligned} u &= A\cos(m\pi x/L)\cos n\theta\cos\omega t \\ v &= B\sin(m\pi x/L)\sin n\theta\cos\omega t \\ w &= C\sin(m\pi x/L)\cos n\theta\cos\omega t \end{aligned} \qquad (2)$$

where *A*, *B* and *C* are arbitrary constants for a given set of *m*, *n* and the angular frequency ω (which is the natural frequency here). These displacements automatically fulfil the shear-diaphragm boundary conditions of zero tangential and radial displacement and zero bending moment and longitudinal membrane force at the cylinder ends. Substitution of solutions (2) into the equations of motion (1) gives a characteristic equation of the form

$$\Omega^6 - K_2\Omega^4 + K_1\Omega^2 - K_0 = 0 \qquad (3)$$

where $\Omega^2 \equiv \rho(1-\nu^2)a^2\omega^2/E$. This is a cubic in Ω^2 and so is easily solvable. The coefficients are given by the expressions

$$\begin{aligned} K_2 &= 1 + \tfrac{1}{2}(3-\nu)(n^2+\lambda^2) + k(n^2+\lambda^2)^2 \\ K_1 &= \tfrac{1}{2}(1-\nu)\left[(3+2\nu)\lambda^2 + n^2 + (n^2+\lambda^2)^2 + \frac{(3-\nu)}{(1-\nu)}k(n^2+\lambda^2)^3\right] \\ K_0 &= \tfrac{1}{2}(1-\nu)\left[(1-\nu^2)\lambda^4 + k(n^2+\lambda^2)^4\right] \end{aligned} \qquad (4)$$

where $\lambda \equiv m\pi a/L$ and $k \equiv h^2/12a^2$.

Since equation (3) is cubic in Ω^2, there are three distinct solutions for the natural frequency for each combination of *m* and *n*. The nature of the corresponding modes can be determined by substituting the three natural frequencies in turn back into the matrix equations that stem from using solutions (2) in the equations of motion (1), to calculate the mode shapes. As is normal in eigenvalue problems, this results in linear dependence between the three equations, and one must be discarded, the final results being relative ratios between the amplitudes of the displacements. One possible expression is

$$\begin{bmatrix} -\lambda^2 - \dfrac{(1-\nu)}{2}n^2 + \Omega^2 & \dfrac{(1+\nu)}{2}\lambda n \\ \dfrac{(1+\nu)}{2}\lambda n & -\dfrac{(1-\nu)}{2}\lambda^2 - n^2 + \Omega^2 \end{bmatrix} \begin{bmatrix} \dfrac{A}{C} \\ \dfrac{B}{C} \end{bmatrix} = \begin{bmatrix} -\nu\lambda \\ n \end{bmatrix} \qquad (5)$$

If A/C and B/C are both less than one, then the mode is predominantly radial (flexural). If A/C is large and B/C small, then the mode is predominantly longitudinal (axial), while a small A/C and large B/C implies a predominantly circumferential (torsional) mode. The radial mode usually has the lowest natural frequency in the group of three.

EXPERIMENTAL SETUP

The cylindrical shell examined in this paper is shown in Figure 2. It is made of 2mm thick mild steel, 1500mm long with a 400mm diameter. End plates 20mm thick are bolted with 8 bolts each to annular flanges of the same thickness which are welded to the cylinder's ends. Two eyelets are also welded to the cylinder to suspend it via a roof crane and sling as shown. The shell part has a longitudinal welded seam running between the hooks. The two edges of the seam meet at a slightly obtuse angle rather than being tangential, so there is some disruption to the circular symmetry of the shell in practice. The cylinder is marked with a grid of 320 points with 20 points around the circumference (about 63mm circumferential spacing) and a longitudinal spacing of 100mm. This gave sufficient spatial resolution to ensure the accurate capture of higher-order modes that may have been present.

The cylinder was excited axially by means of a Gearing and Watson GWV6 30N modal shaker. This was mounted inside the cylinder on a rod welded to one of the end plates as depicted in Figure 3. The shaker is bolted to its bracket via some rubber mounts, to minimise vibration transmission to the end plate via that path. Also mounted on the rod is a cooling blower; however, this was only run intermittently between measurements, to avoid spurious vibration excitation. The main vibratory input path to the end plate is via the stinger shown, which is connected to a PCB 208A02 11.8mV/N force transducer. The mass of the driven endplate-flange assembly with shaker, blower and bolts is approximately 26.3kg and that of the plain endplate and flange with its bolts is about 16.6kg. The mass of the cylindrical shell itself is about 29.4kg.

Normally, a modal shaker would be mounted separately from the structure it excites and the only connection would be via the stinger. The shaker was mounted internally in the manner described above to avoid having external protuberances which could interfere with the sound radiation, and also to test a configuration that would be suitable for future underwater sound radiation measurements where the shaker would necessarily have to be kept dry. In the mounting scheme employed, there must be a reaction force acting along the rod in opposition to the shaker force applied to the centre of the end plate. This results in a degree of moment excitation in addition to the axial force excitation desired. This could be expected to have some effect on the cylinder's motion in spite of the relative rigidity of the end plate and the flange it is bolted to. An alternative to avoid the moment excitation would be to use a centrally mounted inertial shaker, which could still be placed inside the cylinder. However, no inertial shakers were available at the time of the measurements described.

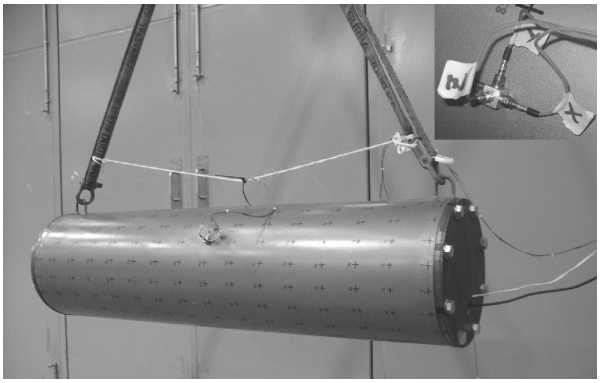

Figure 2. The cylinder suspended by the crane sling, showing the end plates bolted on and the triaxial accelerometer.

Figure 3. The driven end plate, showing (top to bottom) the blower, shaker, stinger and force transducer at the centre of the plate. Access for leads is by three extra holes in the plate.

Also shown inset in Figure 2 is the triaxial accelerometer composed of three 10 mV/ms^{-2} PCB 352C66 accelerometers mounted on an aluminium cube of side length 10mm. This was secured to the cylinder with wax and aligned to measure the accelerations in the longitudinal (x), tangential (y) and radial (z) directions. The accelerometer assembly has a total mass of only 11.2 gram. The light rope shown running between the two ends of the sling was used as a support for the accelerometer cables to be tied to so that their weight did not pull the accelerometer block off the shell. This triaxial accelerometer was moved from point to point marked on the cylinder to measure the three frequency-response functions (FRFs) with a random noise shaker input signal. The FRFs were obtained from the output signals of the accelerometers and force transducer using an HP 3566A FFT analyser controlled by a notebook PC which also stored the data. To obtain clean FRFs, ten averages were taken for each point and a Hanning window was applied to the data.

MEASUREMENTS AND MODES

A typical set of three FRFs measured at one point, number 158, is given in Figure 4. This point is close to the position of the triaxial accelerometer shown in Figure 2. It is interesting to note that the longitudinal (or axial) response has just a few large peaks, while the tangential and especially the radial responses have much higher modal density. This is despite the excitation being in the axial direction only. With random excitation, the input force was a constant level for the entire bandwidth considered. Thus reasonable amounts of energy at radial resonance frequencies were injected into the structure, to be converted from non-resonant axial motion to resonant radial motion through the inherent coupling of the curved shell. The relative importance of this phenomenon in the case where the axial excitation is of a harmonic rather than a broadband nature would have to be determined.

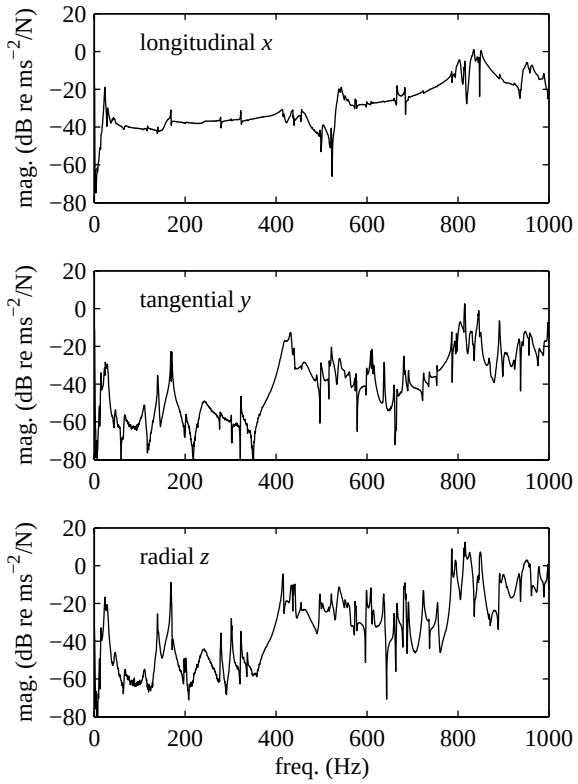

Figure 4. The magnitudes of the FRFs measured in the *x*, *y* and *z* directions at point 158 on the cylindrical surface.

The FRFs measured over the surface of the cylinder were analysed to extract their modal properties using the ICATS MODENT suite. The general principles of modal analysis and the various methods available are described by Ewins (2000). The approach chosen was the NLLS-1 method of MODENT. This is a non-linear least squares curve-fitting procedure that analyses each FRF individually in turn and then collates the results to give one consistent set of natural frequencies and damping values, and to calculate the mode shapes. This method also requires initial estimates of the modes to be given and this was done using a combination of automatic and manual peak picking from the driving-point response. Figure 5 shows this FRF and numbers for the peaks analysed. The group of closely spaced peaks above 800Hz proved too difficult to separate with this method, the analysis failing to converge in this region.

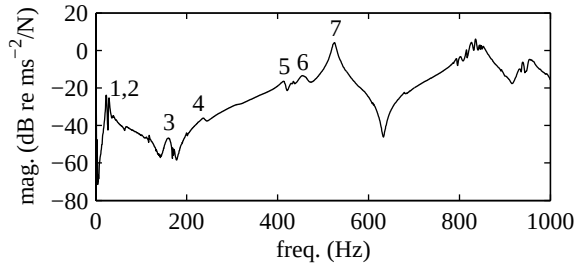

Figure 5. The magnitude of the driving-point FRF measured in the *x* direction on the driven end plate.

The results for the analysed modes are given in Table 1. Animation was used to determination the behaviour of the mode shapes. The mode numbers correspond to the numbers given on the FRF curve in Figure 5. The first two frequencies turn out to correspond to motions where the cylinder acts as a rigid body, in other words, like a rod with no deformation. All the other modes show strong radial motion of various orders. Only mode 7 also shows strong axial motion, which follows from its high peak level on the axial driving response of Figure 5. The other modes show much greater radial and tangential motion than axial motion, which shows up as only small peaks on the driving-point FRF. This confirms the strong effect of the coupling in the cylindrical shell which allows axial excitation to result in large amplitudes of radial and tangential motion.

Table 1. Parameters for some axially prominent modes.

Mode	f_n (Hz)	η_n (%)	m, n	Notes
1	23.9	6.9	0,1	rigid body bounce, driven end moves most
2	29.5	9.1	0,1	rigid body combined bounce and rotation
3	163.3	7.1	1,2	little axial motion
4	202.6	1.8	1,4	little axial motion
5	416.7	2.0	1,1 3,5	combined bending and higher order
6	455.6	2.2	1,1 2,6	combined bending and higher order
7	523.5	1.4	2,2	very strong axial motion

Mode 1 manifests motion in the plane containing both the cylinder's centreline and the line joining the two suspension eyelets. This suggests that it is the result of the cylinder as rigid body supported by the resilience of the crane sling from which the cylinder is suspended. The driven end of the cylinder moves up and down much more than the other end. This suggests the two halves of the sling (divided in the middle by the crane hook) act as independent springs. Axial motion of the driven end induces a change in tension of the half-sling, which being at an angle to the cylinder, also has a vertical component of tension which can act to give this mode. Mode 2 is produced similarly, but has equal up and down motion of the two ends of the cylinder, and also rotates about the attachment points of the eyelets, i.e. it appears to rock side to side about its suspension.

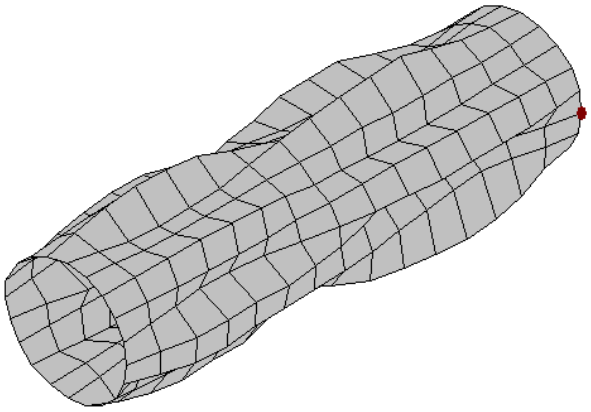

Figure 6. An animation snapshot of mode 6.

Modes 5 and 6 show beam bending ($m = 1$ with the cross-sectional translation of $n = 1$) combined with a higher order deformation. The beam bending is in the vertical plane in the same way as the vertical up and down bouncing motion of the rigid-body modes. In animation, this makes the cylinder look like it is hogging and sagging between its two eyelet suspension points, with the higher-order deformation superimposed on the bending. It is possible that this beam bending is induced by the moment excitation which derives from the way the modal shaker is mounted inside the cylinder. Figure 6 shows an animation snapshot of mode 6. The instant of the snapshot is in the middle of the bending extrema, so the bending is not very clear, but it does indicate the six full waves ($n = 6$) developed around the

circumference, and longitudinally the one full wave (two half waves, $m = 2$) with flattened ends where the cylindrical shell's rotation is constrained by its end caps. The dot indicates the position of measurement point 1, which is next to the suspension eyelet at the driven end of the cylinder.

Mode number 7 with its strong axial motion is illustrated in the animation snapshot of Figure 7. There is no beam bending, so the cylinder's central axis remains straight. What is clear is the second-order longitudinal motion, with the second-order circumferential motion, which results in an appearance of a "squashed" cross-section. What is perhaps most remarkable is the existence of relatively high orders of deformation in these first few noticeable modes of the cylinder assembly. The next step is to determine the effectiveness of these modes in radiating acoustic power.

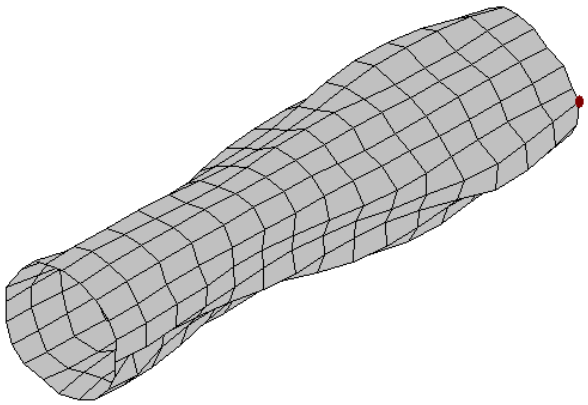

Figure 7. An animation snapshot of mode 7.

The experimentally determined natural frequencies can be compared to the theoretical results determined for a cylinder with shear-diaphragm end conditions as set out by equations (1) to (5). Leissa (1993) notes that the difference between the natural frequencies for a cylinder with shear-diaphragm boundary conditions and one with clamped boundary conditions is primarily due to the moment restraint when $L/a < 1$, but primarily due to the axial restraint when $L/a > 1$, for the case of $a/h = 100$, $\nu = 0.3$ and $m = 1$. For the cylinder under consideration, $L/a = 7.5$ and $a/h = 100$, and since it is made of steel, $\nu = 0.3$. Thus the cylinder falls into the range where the moment restraint alters the natural frequencies from the shear-diaphragm results very little. The thick end plates on the cylinder provide moment restraint, but no axial restraint, although the added mass of the plates does not leave the cylindrical shell completely free in the axial direction. Therefore, the results for shear-diaphragm boundary conditions can give a good estimate for the natural frequencies of this cylinder, especially for modes that are not predominantly axial in nature.

Table 2 compares the natural frequencies of the non-trivial experimental modes with corresponding theoretical results for radial modes calculated from equations (1) to (4), with the roots for Ω^2 converted to frequency in Hz. The frequencies for the radial modes were selected according to the mode-shape parameters A/C and B/C calculated from (5), as described earlier. As an interesting aside, the calculated frequencies for the predominantly torsional modes ranged from 9.8kHz to 26.6kHz for the combinations of *m* and *n* values given in the table, while those for the predominantly axial modes ranged from 5.3kHz to 15.5kHz. These frequency ranges are obviously well outside the frequency range considered in the experimental measurements, and illustrate that the radial mode resonances are much more significant than the other two types at lower frequencies for higher *n* values.

Table 2. Comparison of experimental modes to theory.

Mode	f_n (Hz) expmt	*m*, *n*	f_n (Hz) theory	Percent. diff.
3	163.3	1,2	161.1	–1.3%
4	202.6	1,4	200.7	–0.9%
5	416.7	3,5	404.3	–3.0%
6	455.6	2,6	458.8	+0.7%
7	523.5	2,2	547.2	+4.5%

The results in Table 2 show that the calculated natural frequencies are very close to the measured ones. Thus the simple formula for a cylindrical shell with shear-diaphragm boundary conditions is sufficiently accurate to predict the natural frequencies for the modes observed. This is despite the added mass of the end plates and the slight asymmetry introduced by the seam weld along the length of the cylinder.

CONCLUSIONS

The results presented in this paper have shown that circumferential mode terms of order higher than $n = 0$ have to be considered to give an accurate picture of the dynamics of a cylindrical shell even under axial excitation which is nominally axisymmetric. With a uniform distribution of input force over the frequency bandwidth, radial displacement modes are excited for higher *n* despite there being no strong corresponding axial motion at these resonances. Such radial motion, being normal to the surface, is the main source of acoustic radiation from the cylindrical shell.

It was found that the measured radial modes of the cylinder could be predicted quite accurately by Donnell-Mushtari shell theory for a cylindrical shell with shear-diaphragm boundary conditions at both ends. Given the relative simplicity of these theoretical results, they could provide a good alternative to more complicated modelling.

Further work will measure the sound power radiation from the cylinder and relate this to the measured FRFs and modes. This will allow the development of computationally efficient radiation expressions based on existing models. These can then be used in trialling active vibration control techniques seeking to minimise the sound radiated in air and eventually in water.

REFERENCES

Blakemore M., Woodhouse J. and Hardie D.J.W. (1999). 'Statistical power-flow analysis of an imperfect ribbed cylinder', *Journal of Sound and Vibration*, 222(5), 813-832.

Blevins, R.D. (1995), *Formulas for natural frequency and mode shape*, Krieger Publishing Company, Malabar, Florida, USA.

Choi S.-H., Igusa T. and Achenbach J.D. (1995). 'Nonaxisymmetric vibration and acoustic radiation of a submerged cylindrical shell of finite length containing internal substructures', *Journal of the Acoustical Society of America*, 98(1), 353-362.

Ewins D.J. (2000). *Modal testing: theory, practice and application*, 2nd edn, Research Studies Press, Baldock, Hertfordshire, UK.

Fuller C.R., Elliot S.J. and Nelson P.A. (1996). *Active control of vibration*, Academic Press, London.

Harari A. and Sandman B.E. (1990). 'Radiation and vibrational properties of submerged stiffened cylindrical

shells', *Journal of the Acoustical Society of America*, 88(4), 1817-1830.

Hodges C.H., Power J. and Woodhouse J. (1985a). 'The low frequency vibration of a ribbed cylinder, part 1: theory', *Journal of Sound and Vibration*, 101(2), 219-235.

Hodges C.H., Power J. and Woodhouse J. (1985b). 'The low frequency vibration of a ribbed cylinder, part 2: observations and interpretation', *Journal of Sound and Vibration*, 101(2), 219-235.

Homm A., Ehrlich J., Peine H. and Wiesner H. (2003a). 'Experimental and numerical investigation of a complex submerged structure. Part I: modal analysis', *Acta Acustica united with Acustica*, 89(1), 61-70.

Homm A., Ehrlich J., Peine H. and Wiesner H. (2003b). 'Experimental and numerical investigation of a complex submerged structure. Part II: sound radiation', *Acta Acustica united with Acustica*, 89(1), 71-77.

Junger M.C. and Feit D. (1972). *Sound, structures, and their interaction*, MIT Press, Cambridge USA.

Leissa A. (1993). *Vibration of shells*, Acoustical Society of America, New York.

Lee J.-H. and Kim J. (2002). 'Sound transmission through periodically stiffened cylindrical shells', *Journal of Sound and Vibration*, 251(3), 431-456.

Marcus M.H. and Houston B.H. (2002). 'The effect of internal point masses on the radiation of a ribbed cylindrical shell', *Journal of the Acoustical Society of America*, 112(3), pt 1, 961-965.

Pan X., Tso Y. and Juniper R. (2005). 'Active modal control of hull radiated noise', *Proc. of ACOUSTICS 2005*, 9-11 November 2005, Busselton, Western Australia.

Ruotolo R. (2002). 'Influence of some thin shell theories on the evaluation of the noise level in stiffened cylinders', *Journal of Sound and Vibration*, 255(4), 777-788.

Rumerman M.L. (2002). 'The effect of fluid loading on radiation efficiency', *Journal of the Acoustical Society of America*, 111(1), pt 1, 75-79.

Sandman B.E. (1976). 'Fluid-loading coefficients for a finite cylindrical shell', *Journal of the Acoustical Society of America*, 60(6), 1256-1264.

Scott J.F.M. (1988). 'The free modes of propagation of an infinite fluid-loaded thin cylindrical shell', *Journal of Sound and Vibration*, 125(2), 241-280.

Solaroli G., Gu Z., Baz A. and Ruzzene M. (2003). 'Wave propagation in periodic stiffened shells: spectral finite element modeling and experiments', *Journal of Vibration and Control*, 9(9), 1057-1081.